Fluid Flow and Reactive Transport Around Potential Nuclear Waste Emplacement Tunnels at Yucca Mountain, Nevada

N.F. Spycher, E.L. Sonnenthal, and J.A. Apps
Lawrence Berkeley National Laboratory, Earth Sciences Div., MS 90-1116, 1 Cyclotron Road, Berkeley, CA 94720, USA

Abstract

The evolution of fluid chemistry and mineral alteration around a potential waste emplacement tunnel (drift) is evaluated using numerical modeling. The model considers the flow of water, gas, and heat, plus reactions between minerals, CO_2 gas, and aqueous species, and porosity-permeability-capillary pressure coupling for a dual permeability (fractures and matrix) medium. Two possible operating temperature modes are investigated: a "high-temperature" case with temperatures exceeding the boiling point of water for several hundred years, and a "low-temperature" case with temperatures remaining below boiling for the entire life of the repository. In both cases, possible seepage waters are characterized by dilute to moderate salinities and mildly alkaline pH values. These trends in fluid composition and mineral alteration are controlled by various coupled mechanisms. For example, upon heating and boiling, CO_2 exsolution from pore waters raises pH and causes calcite precipitation. In condensation zones, this CO_2 redissolves, resulting in a decrease in pH that causes calcite dissolution and enhances feldspar alteration to clays. Heat also enhances dissolution of wallrock minerals leading to elevated silica concentrations. Amorphous silica precipitates through evaporative concentration caused by boiling in the high-temperature case, but does not precipitate in the low-temperature case. Some alteration of feldspars to clays and zeolites is predicted in the high-temperature case. In both cases, calcite precipitates when percolating waters are heated near the drift. The predicted porosity decrease

around drifts in the high-temperature case (several percent of the fracture volume) is larger by at least one order of magnitude than in the low temperature case. Although there are important differences between the two investigated temperature modes in the predicted evolution of fluid compositions and mineral alteration around drifts, these differences are small relative to the model uncertainty and the variability of water compositions at Yucca Mountain.

Key words: numerical modeling, reactive transport, mineral alteration, water chemistry, nuclear waste

1. Introduction

This study investigates coupled thermal, hydrological, and chemical (THC) processes that could take place around waste-emplacement tunnels (drifts) at the potential high-level nuclear waste repository at Yucca Mountain, Nevada. These processes would be driven by heat produced from the decay of radionuclides in waste materials (e.g., Buscheck and Nitao, 1993). As drift temperatures rise above ambient values, interactions are expected to take place between the repository host-rocks and fluids (water moisture and vapor, air, and CO_2) naturally contained in these rocks. Whether such interactions could impact long-term repository performance is one of many questions that must be answered. The effect of these interactions on the composition of water that could potentially seep into emplacement drifts is of particular importance to the assessment of corrosion rates of waste containers and other in-drift engineered systems. Mineral alteration around drifts could also affect the potential migration of radionuclides from the repository. For example, the formation of secondary sorbing minerals could retard transport. On the other hand, mineral dissolution could increase the permeability of flow pathways. The objectives of this study were, therefore, to evaluate the effect of water-gas-rock interactions around

potential waste-emplacement drifts, focussing on the chemistry of percolating fluids, mineral-alteration patterns, and resulting rock-porosity changes. Several scenarios have been investigated elsewhere (Sonnenthal and Spycher, 2001), including possible climate changes and different in-drift designs, geochemical systems, host-rock geologic units, hydrogeologic property sets, and repository operating-temperature modes. Here, we present results of one model and focus on the effect of heat on water-gas-rock interactions around an idealized drift in the main repository host-rock geologic unit.

Depending on the spacing between emplacement drifts and between waste packages, as well as the amount of repository pre-closure ventilation, various heat loads (i.e., energy released to the rock per surface area) can be achieved. In this study, two heat load cases are considered. The first case, referred to as the "high-temperature" operating mode, is predicted to yield temperatures above boiling in the vicinity of the drifts for several hundred years. In the second case, referred to as the "low-temperature" operating mode, temperatures at the drift wall are kept below boiling and the surface of waste containers remains below some temperature design threshold (85 °C). In this study, we attempt to quantify the effects of these alternative temperature regimes on water-rock interactions such that their impact on repository performance can be evaluated.

Finally, it should be noted that the model presented here is an idealization of specific physical processes. As a result of such simplification, the model describes overall changes in space and time within the model domain under assumed physical and chemical conditions, and should not be interpreted as yielding exact predictions of future conditions at any specific repository location or under different initial conditions. The focus here is more on evaluating gen

eral trends with time and relative differences in computed water chemistries and mineral alterations between considered temperature regimes, rather than absolute predictions for each investigated case.

2. General Conceptual Model and Coupled Processes

The potential repository host rocks consist of fractured, welded volcanic tuffs located several hundred meters above the regional water table (e.g., Bodvarsson et al., 1999). These geologic units are unsaturated, with a total water-moisture content typically around 10% (by volume). Most of this water resides in the rock matrix (liquid saturation near 0.9), whereas fractures are thought to contain little water (saturation typically < 0.1). Fracture permeability is several orders of magnitude greater than that of the rock matrix (Bandurraga and Bodvarsson, 1999).

The potential effects of thermal loading on the thermohydrology at Yucca Mountain have been investigated by several authors (e.g., Buscheck and Nitao, 1993; Buscheck et al., 1993; Birkholzer et al., 1999; Tsang and Birkholzer, 1999). Upon heating to boiling conditions (approximately 95 °C at Yucca Mountain), water moisture in the rock boils, and a dry zone develops around the drift (Figure 1). In this zone, the water saturation in fractures declines to zero, whereas the rock matrix may still contain water if the vapor pressure in the tight matrix is significantly lowered by capillary pressure or if the total pressure increases. This zone of dry fractures expands outward for several hundred years, impeding seepage into the drift. It then recedes as the repository cools down, until some point in time when water eventually wets fractures at the drift wall again. After tens of thousands of years, following the nearly complete decay of short-lived radionuclides, temperature eventually returns to ambient values.

During the boiling period, mobilized water vapor travels more rapidly in fractures and condenses in cooler areas away from the drift. The condensate flows back towards the boiling zone (Figure 1) mostly by gravity (drainage) but also through the effect of capillary suction (imbibition), and then boils again. These areas of continuous condensate refluxing are anticipated to be the most affected by water-gas-rock interactions. In contrast, if the rock moisture does not boil, much less water is mobilized. Significant evaporation still takes place such that the processes described for the boiling conditions occur, but to a much lesser extent. However, fractures may never completely dry out. Also, as noted earlier, mineral reaction rates are slower at low temperatures than at high temperatures (by one to two orders of magnitude in the present study). For these reasons, variations in water compositions and mineral precipitation or dissolution amounts are expected to be less pronounced at low temperatures.

Water-rock interactions in the subsurface are strongly affected by the CO_2 dissolved in most natural waters. The effects of heating, boiling, and condensation on CO_2 chemical behavior and its effect on water chemistry and mineral alteration in geothermal systems have been understood for some time (e.g., Drummond and Ohmoto, 1985; Reed and Spycher, 1985; Spycher and Reed, 1989). However, in such studies, the coupled effects of fluid flow and reaction were not considered, and the modeled systems were liquid-saturated. To our knowledge, only a few investigations have attempted to model coupled THC processes in an evolving, boiling, unsaturated system. In Xu et al. (2001), we presented preliminary results of such simulations involving multicomponent reactive transport in a dual-continuum model. These simulations captured most of the coupled processes discussed here, including reactive CO_2 transport around a heater-test drift at Yucca Mountain. Lichtner and Seth (1996) simulated such processes around a potential re

pository at Yucca Mountain and predicted pH trends (caused by CO_2 transport) similar to those discussed below. Their study considered a simple model (one-dimensional, single porosity) with a limited number of minerals and chemical components. Nitao (1997) presented another modeling study of coupled THC processes around a repository drift (two-dimensional, dual porosity) that included only silica phases and ignored the effect of reactive CO_2 transport. In a similar study with a more complex chemical system, Glassley (1997) investigated mineral alteration around drifts, including the effect of CO_2 partial pressure, using a limited model (single porosity, liquid-saturated system without gas transport). Here, we consider a two-dimensional, unsaturated dual-continuum model including all major host-rock minerals, several possible secondary solid phases, and reactive CO_2 transport.

Two underground thermal tests at Yucca Mountain have provided the basis to further evaluate the coupled effects of thermal and hydrological processes on water chemistry and mineral alteration, including CO_2 transport, in a boiling unsaturated environment. The Drift Scale Test, and to a lesser extent the Single Heater Test, have provided a significant amount of water chemistry and mineralogical data to understand and model coupled THC processes around a heated drift (Sonnenthal et al., 1999, 2000, 2001, and in preparation; Sonnenthal and Spycher, 2001; Spycher et al., 1999; Xu et al., 2001). From these and earlier studies, the following important processes affecting water and gas compositions have been observed:

- Upon heating (before boiling), pore water evaporates and CO_2 from dissolved inorganic carbonate species naturally present is volatilized. This is typically accompanied by calcite precipitation (i.e., $Ca^{2+} + 2HCO_3^- \Rightarrow CaCO_{3(s)} + CO_{2(g)}\uparrow + H_2O$) and generally also a pH increase in the remaining solution (e.g., $HCO_3^- + H^+ \Rightarrow CO_{2(g)}\uparrow + H_2O$). Eventually, evapora

tive concentration results primarily in the precipitation of amorphous silica and gypsum (or anhydrite) in addition to calcite.

- Upon boiling, the effects are similar to, but more pronounced, than those described above, with increased mobilization of steam and CO_2. Also, upon continuous boiling, steam displaces air and CO_2 in the gas phase.

- In condensation zones, dilution of ambient pore waters is typically accompanied by a pH decrease resulting from the dissolution of CO_2 gas mobilized with steam (e.g. $CO_{2(g)} + H_2O \Rightarrow HCO_3^- + H^+$). This causes silica phases and calcite in fractures to dissolve.

Although these processes are noticeable over the relatively short time scales of the thermal tests (1 to 4 years), additional interactions are likely to affect water compositions around waste emplacement drifts over thousands of years. For example, the precipitation of small amounts of secondary minerals such as clays or zeolites could have a significant effect on water chemistry, although precipitated amounts are too small to be discernable in a short time-frame experiment. To fully understand and predict interactions over longer time frames, numerical models then become a necessity.

3. Modeling Approach

To simulate the complex interactions described above, the following processes were considered: flow of heat, water, and gas (vapor and air, with decoupled CO_2 transport in the vapor/air mixture); reactions between minerals, aqueous species, and CO_2; and porosity-permeability-capillary pressure coupling. In addition, a dual permeability model was used to take into account disequilibria and transport between fractures and the rock matrix (DCCM model as defined in Lichtner, 2000). The multicomponent reactive transport code TOUGHREACT (Xu and Pruess, 2001) was used. This code was further enhanced (Sonnenthal and Spycher, 2001) to

handle the specific unsaturated and boiling conditions expected for the potential repository at Yucca Mountain. TOUGHREACT has been tested and validated against analytical solutions, laboratory experiments, and field thermal tests (Sonnenthal et al., 1999, 2000, 2001, and in preparation; Sonnenthal and Spycher 2001; Xu et al., 2001; Spycher et al. 1999; Dobson et al., this issue). Details on the coupled processes modeled can be found in these studies.

Simulations were performed using a vertical 2-D mesh for a drift spacing of 81 m and a drift radius of 2.75 m. With rock properties laterally homogeneous between drifts, this setup can be viewed as a series of symmetrical, identical half-drift models with no-flux (heat, fluid, chemical) vertical boundaries between them. Accordingly, the numerical mesh was reduced to a half-drift model with a width corresponding to the midpoint between drifts (Figure 2). Geologic data from the 3-D site-scale model (Wu et al., 1999) were used as a basis to map geologic contacts onto the 2-D mesh. The modeled stratigraphy corresponds to a column located near the center of the potential repository. The drift is located in the lower lithophysal hydrogeologic unit of the Topopah Spring Tuff (Tptpll, anticipated to host the majority of the potential repository). The area extending approximately 50 meters above the drift was finely gridded to capture THC effects affecting seepage in the vicinity of the drift. Outside the drift, the smallest grid spacing was specified at the drift wall (20 cm) and increases gradually outward.

Top and bottom boundary conditions were set according to those appropriate for a location near the repository center. The model top was located at the bedrock-alluvium contact near the ground surface (364 m above the potential repository level). A stepwise changing infiltration rate, constant temperature, pressure, and gas saturation (representing open atmosphere), and constant CO_2 partial pressure and composition of infiltrating water were applied at this boundary.

The varying infiltration rate corresponds to possible future mean climate conditions, including present day, monsoon, and glacial transition periods (infiltration steps of 6, 16, and 25 mm/year for 0–600, 600–2000, and >2000 years, respectively) (e.g. Ritcey and Wu, 1999). The bottom boundary was located at the water table (353 m below the repository), with a constant temperature, pressure, and liquid saturation representing saturated conditions. Although this boundary cannot capture possible future water table movements, such fluctuations are anticipated to remain far enough below the repository to have no significant effect on model results at the drift level.

The drift was modeled with a wall closed to gas and water advection but open to heat transfer and to CO_2 gas diffusive transport. Because the drift acts as a capillary barrier, flow into the drift is not predicted to occur even at infiltration rates significantly higher than the rates considered here (Birkholzer et al., 1999). Heat was introduced into the drift through a waste package element (Figure 2) by specifying heat-generation values as a function of time for this element. The two simulated heat loads included the effect of heat removal by ventilation during preclosure (70% removal for the first 50 years in the high-temperature case and 80% removal for the first 300 years in the low-temperature case). Conductive heat transport was computed from the waste package to the drift wall, using time-varying effective thermal conductivities accounting for radiative and convective transport in open areas of the drift. Simulations under ambient conditions (no heat load) were also conducted to serve as a baseline for comparisons with the high- and low-temperature cases.

The initial water was assumed to have the same chemical composition in the rock matrix and fractures (Table 1). The same water re-equilibrated at the temperature of the top model boundary was assumed for infiltration. At the start of this study, these data were the only nearly

complete pore-water analyses for samples collected from a potential repository unit near the potential repository (ultracentrifuged from core taken in Alcove 5 in the Engineering Studies Facility). Iron, aluminum, and total aqueous carbonate concentrations (hereafter listed as HCO_3^-) were not measured and were calculated as shown in Table 1. Studies are currently ongoing to evaluate the model sensitivity to other input water compositions.

Minerals and chemical aqueous components considered in this study are shown in Table 2. Aqueous species and gases were considered in equilibrium with each other. Minerals were assumed to react at equilibrium or under kinetic constraints (Table 2). Initial mineral abundances were derived from XRD measurements on cores (Carey et al. 1997) and analyses of fracture surfaces (Carlos et al., 1993; Levy et al., 1998). Amounts of minerals observed, but present in quantities below the detection limit (typically around a percent for XRD), were estimated. Potential secondary minerals (i.e. those allowed to precipitate but which may not necessarily form) were determined from field observation of thermal alteration (e.g. Vaniman et al., 2001), and by running multicomponent heterogeneous equilibrium simulations of water-rock interaction (e.g. Spycher and Reed, 1989) whereby the stable mineral assemblage at each reaction step was calculated from a large list of possible minerals (after suppressing phases known not to form under ambient pressures and low temperatures). Kinetic and thermodynamic data were taken from numerous literature sources (Sonnenthal and Spycher, 2001). Activity coefficients for aqueous species were computed using an extended Debye-Hückel equation (Helgeson, Kirkham and Flowers, 1981) providing adequate results, in our case, up to ionic strength around 4.

Hydrogeologic parameters (Ahlers and Liu, 2000) were calibrated by inverse modeling as described by Bandurraga and Bodvarsson (1999). The thermodynamic stability of clay and zeo

lite minerals were adjusted (within their determination errors) such that the initial water composition and pH (Table 1) could be maintained reasonably steady under ambient (no heat load) steady-state flow conditions for thousands of years (Spycher et al., 2000). In our case, originally strongly supersaturated smectites and stellerite were destabilized such that they became nearly equilibrated with the initial solution. An increase of the CO_2 partial pressure at the top model boundary (to reflect soil conditions) as well as adjustments of mineral surface areas (reflecting geometric areas) and rate constants further helped achieving fairly steady water compositions under ambient conditions. No formal calibration of geochemical parameters was conducted besides these adjustments. Further details on the modeling approach and input parameters, including all thermodynamic and kinetic data, are given in Sonnenthal and Spycher (2001).

4. Model Results

Here, we focus on differences between the two operating temperature modes, as simulated with the numerical model presented earlier. In most cases, only results for the fracture medium are presented because the fracture permeability is several orders of magnitude larger than the matrix permeability, and therefore fractures are the main flow pathways around the drift.

4.1. Evolution of Thermohydrology and Water Compositions at the Drift Crown

Temperatures at the drift crown (Figure 3a) initially rise but start dropping after 20 years or so, reflecting the early decay of short-lived radionuclides. This drop is followed by a sharp rise at 50 and 300 years for the high- and low-temperature modes, respectively, corresponding to the end of the pre-closure ventilation periods. The high-temperature mode results in boiling, and fractures around the drift wall are predicted to dry out for approximately 1,600 years. After this time, the

drift crown starts to rewet (Figure 3a and 3b). The spatial extent of dryout around the drift depends on the infiltration rate and repository host-rock thermal properties. Above the drift, dryout is predicted to extend approximately 6 to 12 m from the drift center in both the rock matrix and fractures. The boiling front is predicted to expand for approximately 600 years, then to recede after this time. In contrast, in the low-temperature case, rocks around the drift are not predicted to dry out (Figure 3a and 3b), significantly reducing the effect of evaporative concentration around the drift. The greater mobilization of water vapor in the high-temperature case, caused by boiling, results in a temporary higher liquid influx in fractures towards the drift crown at the time of rewetting, compared to the low-temperature case (Figure 3c). However, in both cases, this influx is small and of the same order of magnitude as ambient fluxes.

For the cases considered here, the most visible effect of increasing temperature on water chemistry is the volatilization of CO_2 from the pore water. Upon heating, CO_2 exsolved from matrix water is transported into fractures. In fractures, this generally causes the CO_2 partial pressure to rise above ambient values, accompanied by a pH decrease (Figures 4a and 4b). However, during the dryout period in the high-temperature case, CO_2 concentrations at the drift wall fall largely below ambient values as the result of boiling and displacement by steam (Figure 4a). After an initial drop at the onset of dryout, the CO_2 concentration at the drift crown temporarily increases (it remains, however, still below ambient values), resulting from increased diffusion towards the drift caused by the continued temperature rise after the fractures initially dry out. During early rewetting of fractures at the drift crown, the CO_2 partial pressure in the higher-temperature case is still depressed relative to the lower-temperature case, causing predicted pH values approximately 0.4 units higher than in the lower-temperature case. The volatilization of

CO_2 causes total aqueous carbonate concentrations at the drift wall (not shown here) to decrease below ambient values in fractures by a factor of approximately two in the low-temperature case and approximately four in the high-temperature case.

For most major cations and anions, except aqueous carbonate species, initial concentrations predicted in fractures at the drift crown at the time of rewetting (near 1,600 years) in the high-temperature case are significantly larger (one or more orders of magnitude) than concentrations predicted in the low-temperature case, which do not depart significantly from ambient values (e.g., chloride in Figure 4c). This is primarily the result of greater evaporative concentration resulting from boiling. In fractures, at liquid saturations on the order of the residual saturation (here assumed as 0.01), the salinity of rewetting fluids at the drift crown is predicted to reach a few thousand mg/L in the high temperature case.

The predicted evolution of water composition in fractures at the drift crown, for each temperature case, was also examined using Piper diagrams (Figures 5). In these diagrams, points are shown for selected times and corresponding predicted temperatures, and represent relative rather than absolute concentrations. A larger variability in composition is predicted in the high-temperature case than in the low-temperature case, as would be expected. The effect of CO_2 volatilization caused by the temperature increase, discussed earlier, is clearly shown by the progressive decarbonation of the waters as they undergo heating (lower right triangle on Figures 5a and 5b), then return to ambient values as the temperatures cool. Except for the large depletion of aqueous carbonate during the heating period, the scatter in predicted relative concentrations of major aqueous constituents falls largely within the variability of potential initial pore-water compositions (e.g., Yang et al., 1996).

Under ambient conditions, water compositions are predicted to evolve with time from a somewhat more calcium-dominant character to a somewhat more sodium-dominant character (Figure 5a). This is the result of calcite precipitation and feldspar dissolution. After the thermal perturbation, temperatures and concentrations return to nearly ambient values within the simulated time period (100,000 years). This would indicate no long-lasting (>100,000 years) effects from the thermal perturbation on predicted fluid compositions around the drift. This would also imply that the long-term composition of fluids around the drift should be largely dominated by the composition of infiltrating water (assumed, in the present case, to be similar to the initial pore water), regardless of the operating temperature mode of the repository.

4.2. Predicted Mineral Alteration

The calculated amounts of minerals dissolved and precipitated around the drift are small, and the porosity decreases around the drift for both temperature regimes. In the high-temperature case, mineral precipitation is most pronounced in an area delineating the maximum extent of the dryout zone approximately 10 m above drift center. The total volume of precipitated minerals amounts to several percent of the initial fracture void volume. Most of this porosity decrease is caused by amorphous silica precipitation (Figure 6). This mineral forms primarily at the boiling front from approximately 300 to 2,000 years, corresponding to the period starting when the front approaches a stationary state (when it is farthest from the drift) until the front has receded to the drift wall. Gypsum (no more than a few percent of the fracture volume) and much smaller amounts of fluorite (< 0.1 %) also precipitate in this zone during the same period, but dissolve rapidly upon rewetting. The increased infiltration rate at the surface at 600 years (from 6 to 16 mm/year) causes a rapid downward shift of the boiling front at approximately 750 years, causing

a gap in the pattern of silica deposition around the drift (Figure 6). Note that the calculated amorphous silica amounts shown here are from a more recent simulation than others presented in this paper. In this simulation, silica deposition is modeled using a more refined treatment of precipitation at the boiling front than in earlier simulations. Amorphous silica precipitation is supplanted at later times by calcite precipitation (Figure 7a). Calcite, having a retrograde solubility, is deposited primarily when infiltrating waters, replenished in aqueous carbonate and calcium, are heated as they percolate back towards the drift where elevated temperatures remain for several tens of thousands of years. It should be mentioned here that the irregular calculated mineral precipitation patterns shown on figures 6 and 7a are numerical effects resulting from high precipitation rates and a flow direction oblique to the grid orientation; although results would be smoother without such effects, predicted general mineral patterns and amounts would not be affected. Clays, predominantly illite, also precipitate in small quantities mostly in the rock matrix (Figure 7b) as the alteration product of rock-forming feldspars (e.g., $2.33NaAlSi_3O_8$ [albite] + $2H^+$ ==> $Na_{0.33}Al_{2.33}Si_{3.67}O_{10}(OH)_2$ [smectite] + $3.32SiO_2$ + $2Na^+$). Small amounts of stellerite precipitate around the drift (predominantly in the rock matrix) during the initial cooling stage (e.g., 2 $NaAlSi_3O_8$ [albite] + SiO_2 + $CaCO_3$ [calcite] + H^+ + $7H_2O$ <==> $CaAl_2Si_7O_{18} \cdot 7H_2O$ [stellerite] + $2Na^+$ + HCO_3^-), but start redissolving after approximately 5,000 years and eventually dissolve entirely. Precipitation of only negligible amounts of other zeolites is predicted around the drift.

In the low-temperature case, the porosity also decreases, but to a much lesser extent than in the high-temperature case (by an order of magnitude or more). The reaction front is essentially stationary around the drift, compared to the front extending with dryout in the high-temperature

case. As a result, the largest porosity decrease occurs in a small band (< 1 m) directly around the drift wall, caused almost entirely by calcite precipitation (Figure 8a), due both to the temperature increase and to CO_2 degassing. Some amorphous silica precipitates at the bottom of the drift (closest to the waste package) as the result of evaporative concentration. However, in contrast to the high-temperature case, essentially no amorphous silica precipitation takes place upon cooling because of the lack of a boiling front. Some clay alteration is predicted, mostly in the matrix and in amounts that are smaller than predicted for the high-temperature case (Figure 8b). No stellerite precipitation is predicted.

5. Uncertainties in Model Results

Because of the large number and variability of input parameters, as well as the complexity of modeled THC processes, a rigorous quantification (in a statistical sense) of model uncertainty is not achievable (i.e., computation speed is too limited for investigations such as Monte-Carlo analyses). For this reason, the uncertainty of simulations such as those presented here can only be evaluated qualitatively, with the goal on narrowing rather than quantifying uncertainty. Increasing the confidence in model results relies strongly on model validation against field and experimental data. Such a validation effort is ongoing. However, the length of time for which test data are available (currently 4 years for the Drift Scale Test) is short compared to the time frame under consideration (thousands of years), thus limiting our predictive confidence over such long periods of time. Some important uncertainties have been investigated (Sonnenthal and Spycher, 2001; BSC, 2001). Although many uncertainties were identified, only a few may dominate the overall uncertainty of the predicted water compositions. These include kinetic and thermodynamic data, initial and infiltration-water compositions, secondary mineral phases included in

simulations, and trace primary mineral phases (and related aqueous species) included in simulations. Uncertainties regarding infiltration rates are also important. However, at high infiltration rates (more conducive to in-drift seepage than at low infiltration), calculated concentrations are more a function of transport than reaction, such that the prediction uncertainty becomes more directly related to the assumed composition of infiltration water and less dependent on rates of reaction (for slow-reacting minerals) or infiltration.

Uncertainties in the formulation of modeled processes are another source of overall model uncertainty. For example, the lowering of water vapor pressure caused by capillary pressure in the rock matrix and by water salinity is not taken into account here, which could result in overpredicting the size of the dryout zone and the amount of evaporative concentration. Another important source of uncertainty is the dual-continuum formulation. As implemented in the model, this approach does not resolve concentration gradients within the matrix at each grid node. Therefore, it may not be accurate (Lichtner, 2000). However, fracture-matrix connection areas needed to implement any dual-continuum approach are largely uncertain, and may contribute more to the model uncertainty than the dual-continuum formulation itself. In our case, the model reproduces reasonably well the trends of CO_2 gas and aqueous species concentrations measured in the Drift Scale Test. For this reason, we believe it provides a reasonable approximation of chemical exchanges between fractures and matrix.

Finally, heterogeneities in the host-rock around the drift may further increase the model uncertainty. To evaluate the effect of heterogeneity on our model, additional simulations were conducted for three realizations of heterogenous fracture permeability around the drift (Sonnenthal and Spycher, 2001). These indicated an increased potential for localized fracture sealing (at

a centimeter to meter scale) due to flow focussing, but general patterns of flow, water compositions, and mineral alteration similar to those presented here.

6. Discussion and Conclusions

Important differences in fluid compositions and mineral alteration are predicted between the two considered operating-temperature modes. However, in both cases, the effect of the thermal pulse on water chemistry around the drift is relatively small when examined in context with the model uncertainties and notably the variability in ambient pore-water compositions at Yucca Mountain. In both temperature cases, fracture waters at the drift crown are predicted to exhibit neutral to moderately alkaline pH and salinities typically remaining less than a few thousand mg/L. In the low-temperature case, predicted concentrations generally differ little from initial values. The two main effects of heat on predicted water compositions are decarbonation and evaporative concentration, which are more pronounced at high than at low temperatures. For both the high- and low-temperature cases, the scatter defined by the predicted water compositions at the drift crown over time falls largely (although not entirely) within the variability of water compositions that could be used for input into the model. Higher temperatures increase the variability of predicted concentrations at the drift wall, relative to lower temperatures. However, this effect is predicted to be relatively short-lived. Within 10,000 years after waste emplacement, the general nature of predicted water compositions returns largely to within the range defined by observed ambient compositions. As temperatures decrease and return to ambient values, the predicted water compositions at the drift crown return to ambient values for both temperature cases. Because these results have a large uncertainty, more work is underway to reduce the model uncertainty and evaluate how this uncertainty affects the conclusions drawn here.

Factors that would favor a high-temperature operating mode include the benefit of lower seepage probability during dryout and possible clay and zeolite alteration around drifts. These could hamper the migration of waste constituents (i.e., through limiting the source of water and potentially retarding radionuclides). On the other hand, higher temperatures and boiling could result in high evaporative concentration and, at the time of rewetting, higher liquid fluxes towards the drift than if no boiling took place. Therefore, even though the likelihood of seepage is limited during dryout, the possibility of increased seepage and increased seepage salinity at the time of rewetting in the high temperature case should not be overlooked.

The potential for sealing of fractures around (and mostly above) the drift is greater at high than at low temperatures. Although sealing around the drift could limit seepage onto waste packages, it could also potentially have a detrimental effect on the thermohydrology around drifts. Experimental studies suggest that fracture sealing is not likely, given the model infiltration rates and fracture porosity (Dobson et al., this issue). However, the potential for fracture sealing increases with decreasing fracture porosity (e.g. Lichtner 2000). In our case, for both temperature regimes, an initial fracture porosity of 0.01 was specified based on in-situ gas tracer-test measurements. Using this value, with this model, the predicted amounts of minerals precipitating in fractures did not affect significantly the overall rock permeability and flow patterns around the drift. Therefore, potential negative effects of fracture sealing were not observed. Had the initial fracture porosity been smaller, significant sealing may have been predicted (e.g. Nitao, 1997). Additional modeling work and refinements are underway to investigate further the probability and effect of fracture sealing around the potential repository.

Uncertainties related to water-rock-waste interactions and thermohydrology are smaller at low than at high temperatures. This is viewed as the main advantage of a low-temperature operating mode. However, in order to achieve a smaller heat load (per surface area) for the same mass of waste, the repository footprint would have to be significantly enlarged, thus increasing uncertainties related to spatial heterogeneity in geology, mineralogy, water compositions, and infiltration. Therefore, assessing which temperature mode is most beneficial to the performance of the potential repository cannot be based solely on the model results presented here. Other factors, such as the temperature effect on waste chemistry and waste container corrosion rates, are important and may become deciding factors for which operating mode to pursue.

Acknowledgments

The authors wish to acknowledge Peter Lichtner and an anonymous reviewer for their reviews and constructive comments for improvement of this paper. This work was supported by the Director, Office of Civilian Radioactive Waste Management, U.S. Department of Energy, through Memorandum Purchase Order EA9013MC5X between Bechtel SAIC Company, LLC and the Ernest Orlando Lawrence Berkeley National Laboratory (Berkeley Lab). The support is provided to Berkeley Lab through the U.S. Department of Energy Contract No. DE-AC03-76SF00098.

Figure Captions (Spycher et al., Predictions of Fluid Flow and Reactive Transport...)

Figure 1. Conceptual model of thermohydrological processes around a potential waste emplacement tunnel (drift) for a case where temperatures exceed the boiling point of water. A heat pipe often forms between the dryout and condensation zones as a result of continuous boiling and refluxing of steam condensate towards the boiling front.

Figure 2. Numerical model grid, with the following hydrogeologic units shown: Topopah Spring Tuff Middle Non-Lithophysal (Tptpmn), Lower Lithopysal (Tptpll), and Lower Non-Lithophysal (Tptpln) units. The drift includes various discretized engineered features as shown.

Figure 3. Time profiles of calculated thermohydrologic parameters in fractures at the drift crown: (a) temperature, (b) liquid saturation, (c) vertical liquid flux (towards drift crown). Results are shown for the high-temperature (High T), low temperature (Low T) and ambient cases. Infiltration rate at the top model boundary increases stepwise from 6 to 16 mm/yr at 600 years and from 16 to 25 mm/yr at 2000 years.

Figure 4. Time profiles of (a) modeled CO_2 gas concentrations, (b) pH, and (c) chloride concentrations at the drift crown in fractures. Results are shown for the high-temperature (High T), low temperature (Low T) and ambient cases. For the high-temperature case, the dryout period is left blank (no water); numbers by each curve indicate the last output liquid saturation before dryout and the first output liquid saturation during rewetting.

Figure 5. Piper diagrams showing the modeled evolution of water compositions.
(a) Ambient conditions (no thermal perturbation) (points a-j) and high-temperature case (points A-H). (b) Low-temperature case. Points are plotted for selected time intervals and corresponding temperatures as shown in the legend. The initial water composition (INITIAL) is also plotted and corresponds to the data in Table 1.

Figure 6. Contour plot of amorphous silica volume fraction change at 2000 years, high-temperature case; precipitation of this mineral accounts for most of the porosity reduction around the drift. See text. In the low-temperature case, essentially no silica precipitates due to the absence of a boiling front.

Figure 7. Contour plot of modeled mineral volume fraction change at 20,000 years, high-temperature case. (a) Calcite in fractures. (b) Illite in the rock matrix. See text.

Figure 8. Contour plot of modeled mineral volume fraction change at 20,000 years,
low-temperature case. (a) Calcite in fractures. (b) Illite in the rock matrix. See text.

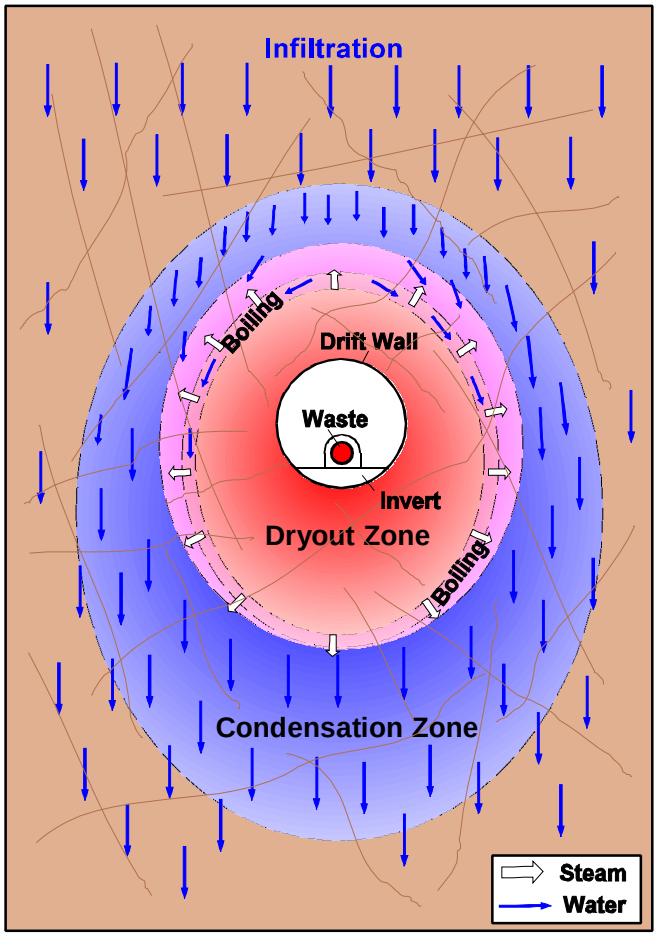

Figure 1. Conceptual model of thermohydrological processes around a potential waste emplacement tunnel (drift) for a case where temperatures exceed the boiling point of water. A heat pipe often forms between the dryout and condensation zones as a result of continuous boiling and refluxing of steam condensate towards the boiling front.

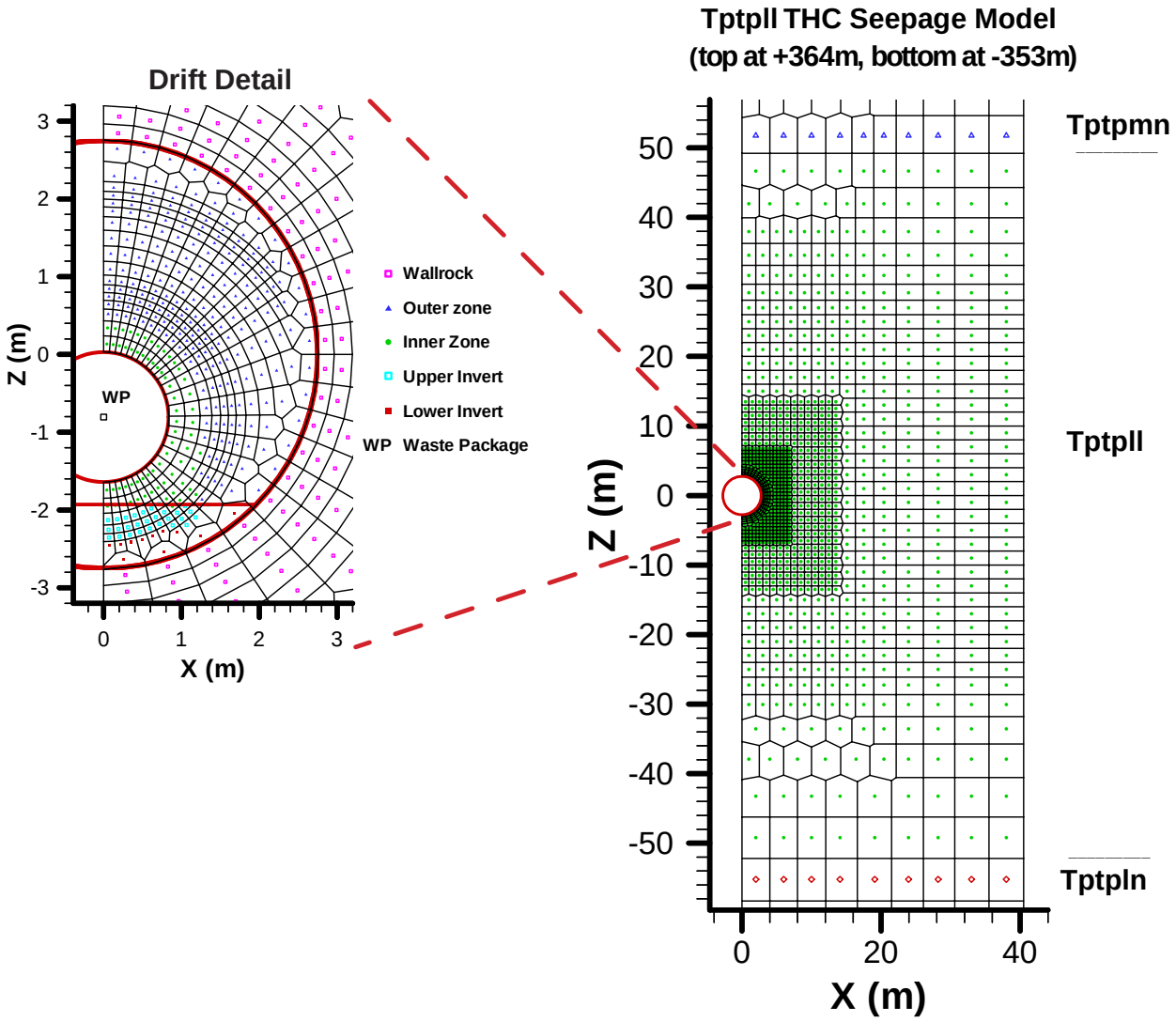

Figure 2. Numerical model grid, with the following hydrogeologic units shown: Topopah Spring Tuff Middle Non-Lithophysal (Tptpmn), Lower Lithopysal (Tptpll), and Lower Non-Lithophysal (Tptpln) units. The drift includes various discretized engineered features as shown.

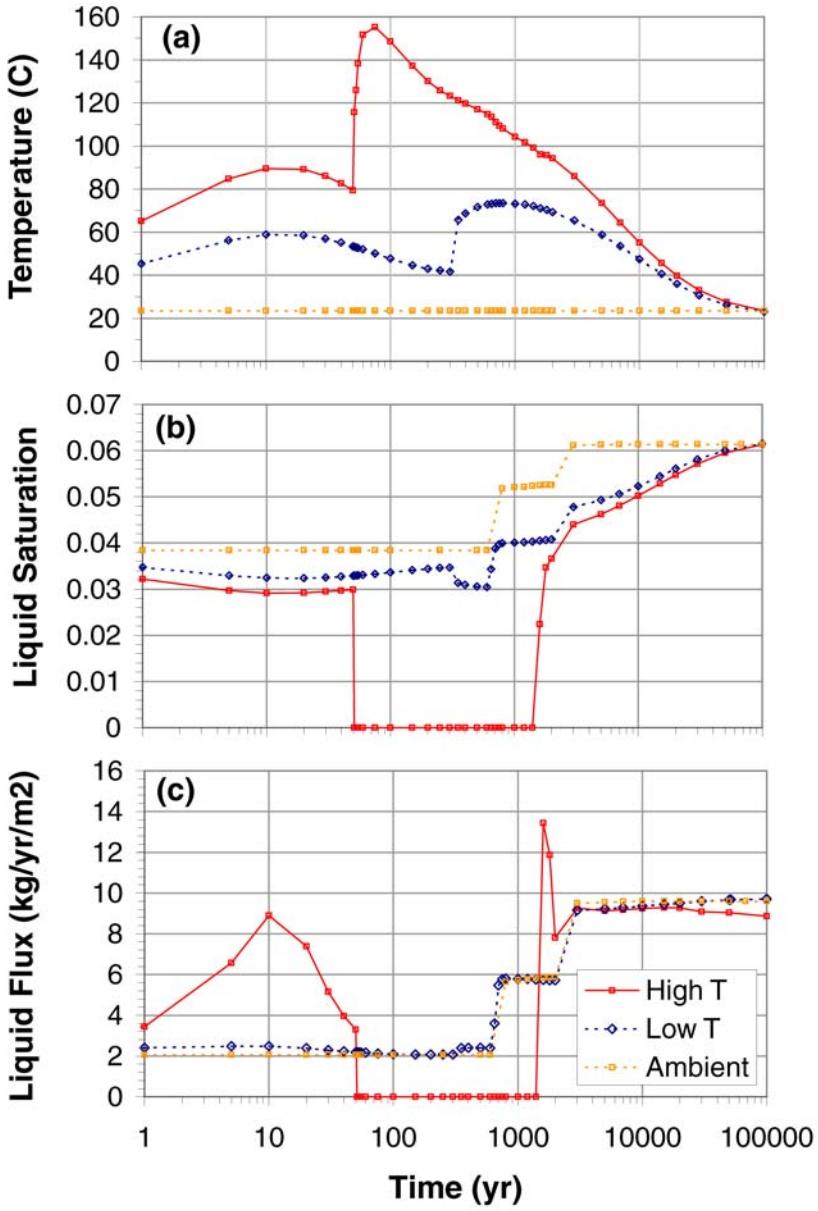

Figure 3. Time profiles of calculated thermohydrologic parameters in fractures at the drift crown: (a) temperature, (b) liquid saturation, (c) vertical liquid flux (towards drift crown). Results are shown for the high-temperature (High T), low temperature (Low T) and ambient cases. Infiltration rate at the top model boundary increases stepwise from 6 to 16 mm/yr at 600 years and from 16 to 25 mm/yr at 2000 years.

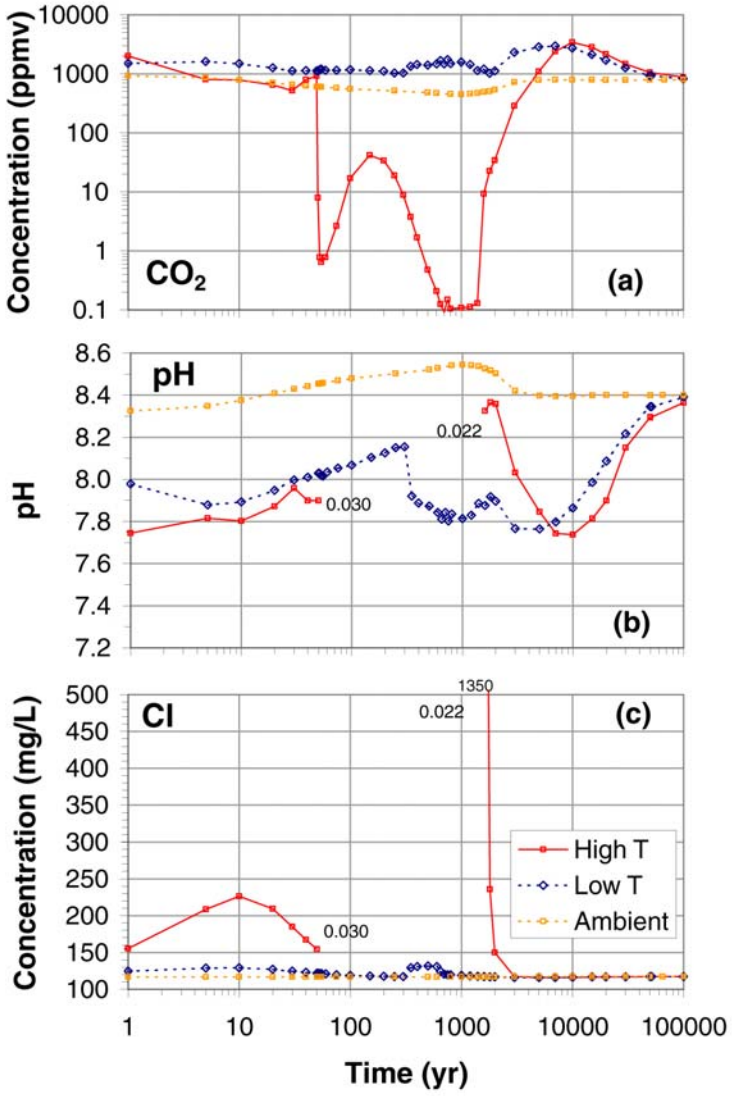

Figure 4. Time profiles of (a) modeled CO_2 gas concentrations, (b) pH, and (c) chloride concentrations at the drift crown in fractures. Results are shown for the high-temperature (High T), low temperature (Low T) and ambient cases. For the high-temperature case, the dryout period is left blank (no water); numbers by each curve indicate the last output liquid saturation before dryout and the first output liquid saturation during rewetting.

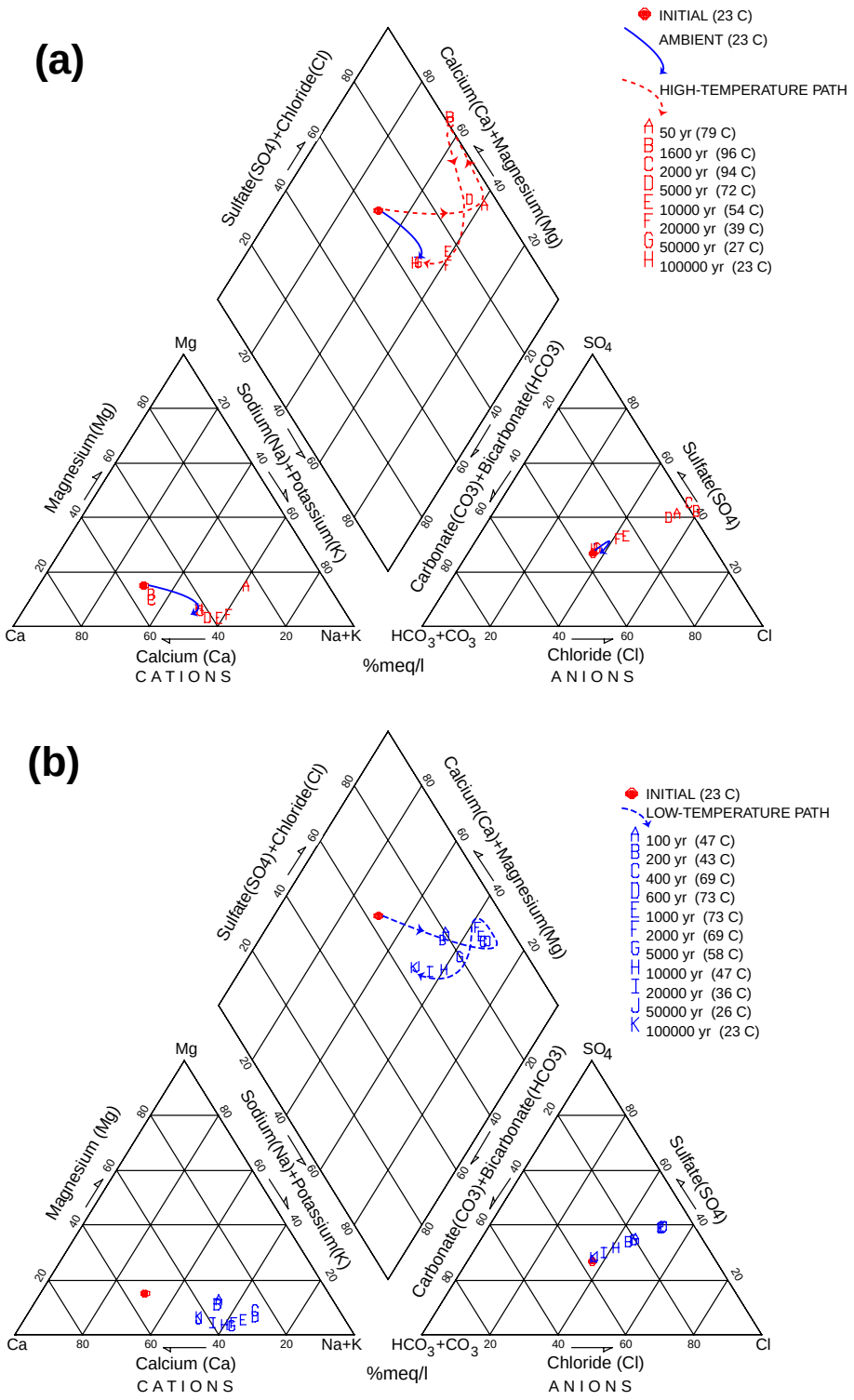

Figure 5. Piper diagrams showing the modeled evolution of water compositions. (a) Ambient conditions (no thermal perturbation) (points a-j) and high-temperature case (points A-H). (b) Low-temperature case. Points are plotted for selected time intervals and corresponding temperatures as shown in the legend. The initial water composition (INITIAL) is also plotted and corresponds to the data in Table 1.

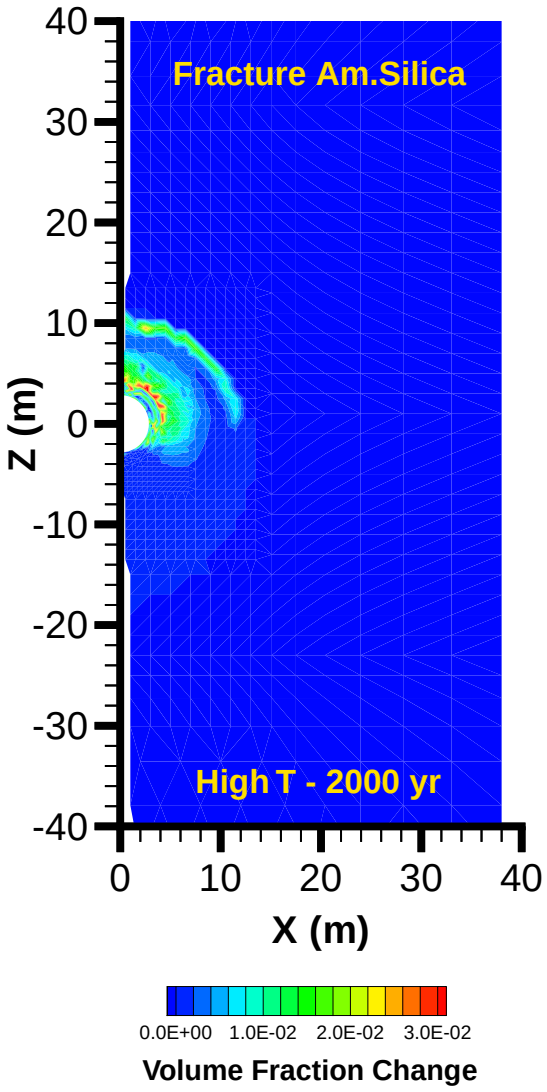

Figure 6. Contour plot of amorphous silica volume fraction change at 2000 years, high-temperature case; precipitation of this mineral accounts for most of the porosity reduction around the drift. See text. In the low-temperature case, essentially no silica precipitates due to the absence of a boiling front.

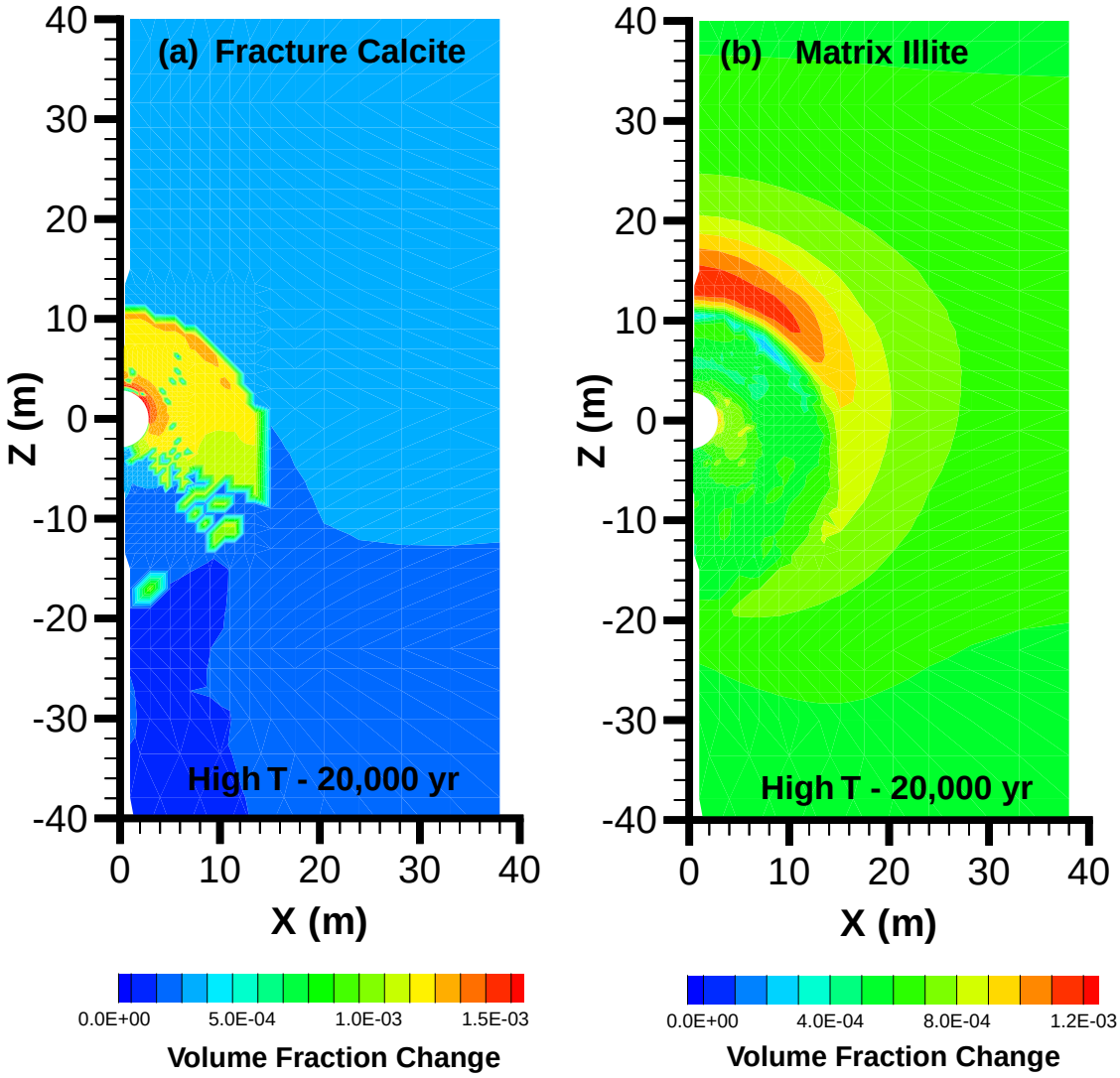

Figure 7. Contour plot of modeled mineral volume fraction change at 20,000 years, high-temperature case. (a) Calcite in fractures. (b) Illite in the rock matrix. See text.

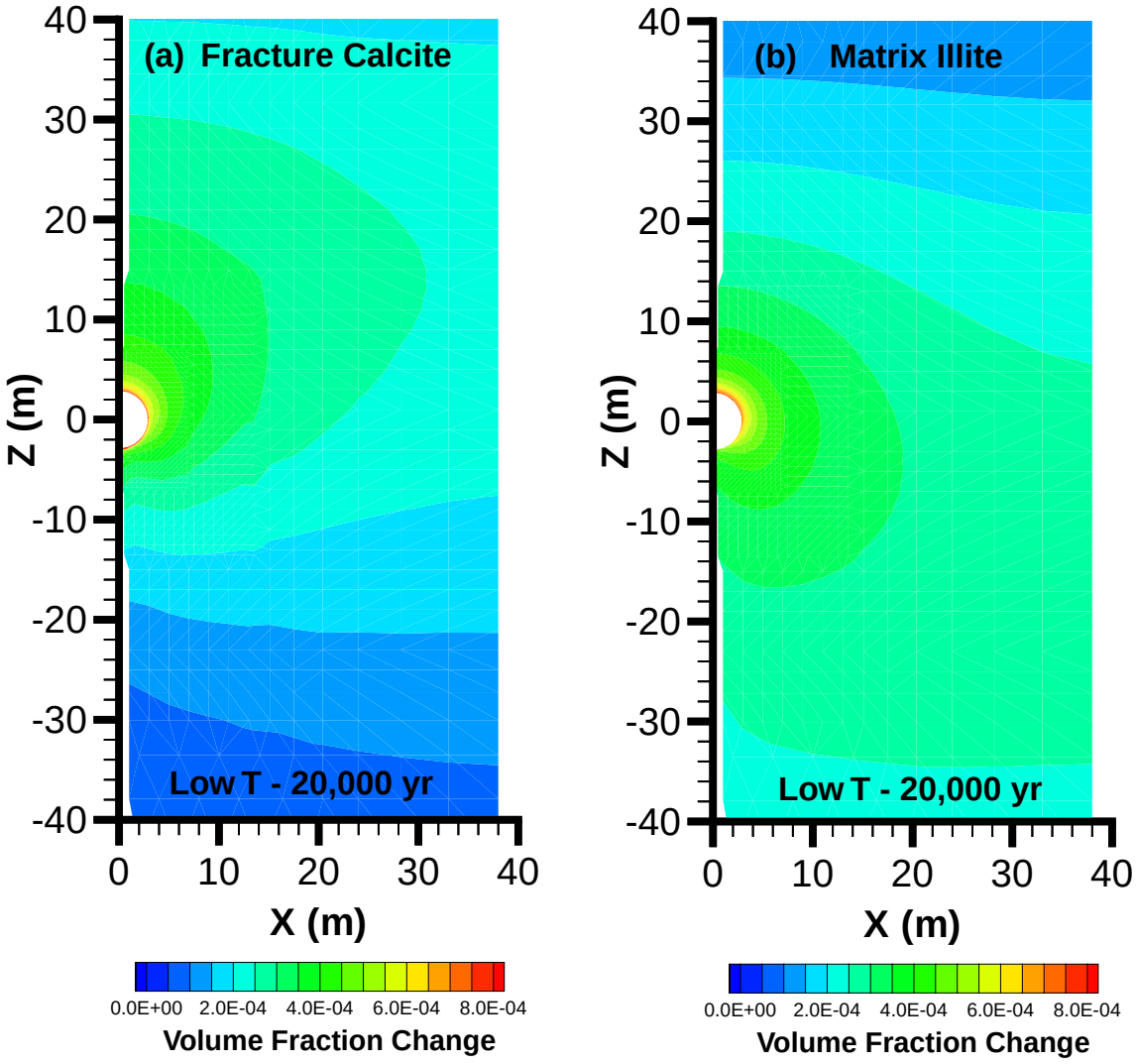

Figure 8. Contour plot of modeled mineral volume fraction change at 20,000 years, low-temperature case. (a) Calcite in fractures. (b) Illite in the rock matrix. See text.

Table 1. Initial Water Composition in Fractures (F), Matrix (M), and Infiltration Waters[1].

Parameters	Units	Concentration	Water
pH	pH Units	8.32 (at 25 C) 7.75 (at 17 C) [2]	F, M I
Na^+	mg/L	61.3	F, M, I
$SiO_2(aq)$	mg/L	70.5	F, M, I
Ca^{2+}	mg/L	101	F, M, I
K^+	mg/L	8.0	F, M, I
Mg^{2+}	mg/L	17	F, M, I
Al^{3+}	mg/L	$1.67x10^{-5}$ [3] $2.64x10^{-6}$ [4]	F, M I
Fe^{3+}	mg/L	$6.46x10^{-8}$ [5] $2.88x10^{-8}$ [6]	F, M I
HCO_3^-	mg/L	200 [7] 216 [2]	F, M I
Cl^-	mg/L	117	F, M, I
SO_4^{2-}	mg/L	116	F, M, I
F^-	mg/L	0.86	F, M, I

NOTES: [1] Average of Tptpmn Porewater Analyses ESF-HD-PERM-2 (30.1'-30.5') and ESFHD- PERM-3 (34.8'-35.1'), unless indicated otherwise below (data sources in Sonnenthal and Spycher, 2001).

[2] HCO_3^- calculated from equilibrium with $\log(P_{CO2}) = -2.5$, and pH adjusted until charge balance was obtained.

[3] Calculated by equilibrating with illite at 25ºC and pH 8.32.

[4] Calculated by equilibrating with illite at 17ºC and pH 7.75.

[5] Calculated by equilibrating with hematite at 25ºC and pH 8.32.

[6] Calculated by equilibrating with hematite at 17ºC and pH 7.75.

[7] Total aqueous carbonate as HCO_3^-, calculated from charge balance.

Table 2. Primary aqueous species (components), minerals, and gases included in simulations. Other known stable aqueous species (34 in this case) derived from the primary components were also considered. Initial mineral abundances in the rocks surrounding the drift are shown (volume % solid), with blank values indicating secondary minerals (italics) not initially present but allowed to form. Glass is not present in modeled geologic units around the drift but occurs in other modeled units. Minerals were assumed to react at equilibrium (Eq) or under kinetic constraints (Kin), with some them only allowed to dissolve (Kin D). See Table 1 for total initial concentrations of aqueous species.

Primary Aqueous Species[1]	**Minerals**	Initial Vol % Matrix	Initial Vol % Fractures	Reaction
H_2O	Calcite	0.04	2	Eq
H^+	Tridymite	2.3	1.5	Kin D
Na^+	Cristobalite-a	19	11	Kin D
K^+	Quartz	14	8.5	Kin D
Ca^{2+}	*Amorphous Silica*			Kin
Mg^{2+}	Hematite	0.2	0.1	Kin D
SiO_2	Fluorite	0.01	0.01	Kin
AlO_2^-	*Gypsum*			Eq
$HFeO_2$	*Goethite*			Eq
HCO_3^-	Albite	26	16	Kin
Cl^-	K-feldspar	35	21	Kin
SO_4^{2-}	Anorthite	0.9	0.5	Kin D
F^-	Ca-Smectite	0.7	2	Kin
	Mg-Smectite	0.7	2	Kin
Gases	Na-Smectite	0.3	0.8	Kin
CO_2	Illite	0.5	1.5	Kin
H_2O	*Kaolinite*			Kin
Air	Opal-CT (proxy)	1	1	Kin D
	Stellerite		32	Kin
	Heulandite	0.002	0.001	Kin
	Mordenite	0.001		Kin
	Clinoptilolite	0.005	0.003	Kin
	Glass[2]			Kin D

References

Ahlers, C.F., Liu H.H., 2000. Calibrated Properties Model. Analysis/Model Report AMR MDL-NBS-HS-000003, REV00. LBID-2325. Lawrence Berkeley National Laboratory, Berkeley California.

BSC (Bechtel SAIC Company) 2001. FY01 Supplemental Science and Performance Analyses, Volume 1: Scientific Bases and Analyses. TDR-MGR-MD-000007 REV 00. Las Vegas, Nevada: Bechtel SAIC Company.

Bandurraga, T.M., Bodvarsson, G.S., 1999. Calibrating hydrologic parameters for the 3-D site-scale unsaturated zone model at Yucca Mountain, Nevada. J. Contaminant Hydrology, 38: 25-46.

Bodvarsson G.S., Boyle, W., Pattersson, R., Williams D., 1999. Overview of scientific investigations at Yucca Mountain - the potential repository for high-level nuclear waste. J. Contaminant Hydrology, 38: 3-24.

Birkholzer, J., Li, G., Tsang, C.F., Tsang, Y., 1999. Modeling Studies and analysis of seepage into drifts at Yucca Mountain. J. Contaminant Hydrology, 38: 349-384.

Buscheck, T.A., Nitao, J.J., 1993. The impact of thermal loading on repository performance at Yucca Mountain: Part I. Modeling and Analysis. Nuclear Technology, 104 (3): 418-448.

Buscheck, T.A., Wilder D.G., Nitao, J.J., 1993. Repository heat-driven hydrothermal flow at Yucca Mountain: Part II. Large-scale in-situ heater tests. Nuclear Technology, 104: (3) 449-471.

Carey J., Chipera, S., Vaniman, D., Bish, D., Viswanathan H., and Carter-Krogh, K, 1997. Three-dimentional mineralogic model of Yucca Moutain, Nevada. Los Alamos National Laboratory, Los Alamos, NM. YMP milestone report SP344BM4.

Carlos, B., Chipera, S., Bish, D., Raymond, R., 1993. Distribution and chemistry of fracture-lining zeolites at Yucca Mountain, Nevada. In: Natural Zeolites '93, D.W.Ming and F.A. Mumpton, eds, pp. 547-563, Int. Comm. Natural Zeolites, Brockport, New York.

Dobson, P.F., Kneafsey, T.J., Sonnenthal, E.L., Spycher, N.F., Apps, J., this issue.

Drummond, S.E., Ohmoto, H., 1985. Chemical evolution and mineral deposition in boiling hydrothermal systems. Economic Geology, 80: 1427-1439.

Glassley, W., 1997. Drift-scale THC scoping calculations and alteration of flow pathways above and below repository drifts. Chapter 5.7 in: Near-field altered zone models report, E.L. Hardin (ed.). YMP Milestone SP3100M4, Lawrence Livermore National Laboratory, Livermore, CA.

Helgesson H.C., Kirkham D.H., Flowers G.C., 1981. Theoretical prediction of the thermodynamic behavior of aqueous electrolytes at high pressures and temperatures: IV. Calculation of activity coefficients, osmotic coefficients, and apparent molal and standard and relative partial molal properties to 600 C and 5 kb. American Journal of Science, 281: 1249-1516.

Lichtner P.C., 2000. Critique of dual continuum formulations of multicomponent reactive transport in fractured porous media. In: Dynamics of Fluids in Fractured Rocks, B.Faybishenko, ed, AGU Monograph, 122:281-298.

Lichtner P.C., Seth, M., 1996. Multiphase-multicomponent nonisothermal reactive transport in partially saturated porous media. Proceedings of the 1996 international conference on deep geological disposal of radioactive waste, Sept. 16-19, Winnipeg, Manitoba. Canadian Nuclear Society.

Levy, S., Chipera, S., Snow, M., 1998. Mineralogical products of the ESF Single-Heater test. YMP Milestone SPY147M4, Los Alamos National Laboratory, Los Alamos, NM.

Nitao J., 1997. Thermohydrochemical alteration of flow pathways above and below the repository. Chapter 5.6 in: Near-field altered zone models report, E.L. Hardin (ed.). YMP Milestone SP3100M4, Lawrence Livermore National Laboratory, Livermore, CA.

Reed, M.H., Spycher, N.F., 1985. Boiling, cooling, and oxidation in epithermal systems: a numerical modeling approach. Rev. Econ. Geol., v.2: pp. 249-272.

Ritcey, A.C., Wu, Y.S., 1999. Evaluation of the effect of future climate change on the distribution and movement of moisture in the unsaturated zone at Yucca Mountain, NV. J. Contaminant Hydrology 38, 257-279.

Sonnenthal E., Spycher, N., 2001. Drift-scale coupled processes (Drift-Scale Test and THC seepage) models. Analysis/Model Report AMR U0110/N0120, MDL-NBS-HS-000001 REV01. LBID-2340. Lawrence Berkeley National Laboratory, Berkeley CA.

Sonnenthal, E.L., Spycher, N.F., Apps, J., Conrad, M., 2001. A Conceptual Model for Reaction-Transport Processes in Unsaturated Fractured Rocks at Yucca Mountain: Model Validation using the Drift Scale Heater Test. LBNL-48292 Abs., Lawrence Berkeley National Laboratory, Berkeley, California (Eleventh Annual V.M. Goldschmidt Conference, Hot Springs, Virginia, May 19-24).

Sonnenthal, E., Spycher, N., Apps J., Conrad M., 2000. Assessment of water-rock and fracture-matrix interaction based on reaction-transport modeling of a large-scale thermal test at Yucca Mountain. Eos Trans. AGU, 81(48): Fall Meet. Suppl., Abstract H52D-10.

Sonnenthal, E., Spycher, N., Apps, J., Simmons, A., 1999. Numerical modeling of coupled thermo-hydro-chemical processes for the in-situ thermal tests at Yucca Mountain, Nevada. *Proceedings of the International Symposium on Dynamics of Fluids in Fractured Rocks:*

Concepts and Recent Advances, in Honor of Paul A.Witherspoon's 80th Birthday. February 10-12, 1999, LBNL-42718, p. 234-237. Lawrence Berkeley National Laboratory, Berkeley CA.

Spycher, N., Sonnenthal, E., Apps, J., 2000. Simulating long-term reactive transport for studies of nuclear waste disposal: establishing steady initial conditions and thermodynamic data calibration. Eos Trans. AGU, 81(48): Fall Meet. Suppl., Abstract H61A-25.

Spycher, N., Sonnenthal, E., Apps, J., 1999. Interpretive analysis of the thermo-hydrological-chemical aspects of the single heater test. Chapter 4 in: Y.W. Tsang; J. App.; J.T. Birkholzer; B. Freifeld; M.Q. Hu; J. Peterson; E. Sonnenthal; N. Spycher, *Yucca Mountain Single Heater Test Final Report*. Yucca Mountain Site Characterization Project. LBNL-42537. Lawrence Berkeley National Laboratory, Berkeley, CA.

Spycher, N.F., Reed M.H., 1989. Evolution of a Broadlands-type epithermal ore fluid along alternative P-T paths: implications for the transport and deposition of base, precious and volatile metals. Economic Geology 84: 328-359.

Tsang, Y.W., Birkholzer, J.T., 1999. Predictions and observations of the thermal-hydrological conditions of the Single Heater Test. J. Contaminant Hydrology, 38: 385-425.

Vaniman D.T., Chipera S.J., Bish D.L., Carey J.W., Levy S.S., 2001. Quantification of unsaturated-zone alteration and cation exchange in zeolitized tuffs at Yucca Mountain, Nevada, USA. Geochimica Cosmochimica Acta, 65:3409-3433.

Wu, Y.S., Haukwa, C., Bodvarsson, G.S., 1999. A site-scale model for fluid and heat flow in the unsaturated zone of Yucca Mountain, Nevada. J. Contaminant Hydrology, 38: 185-215.

Xu, T., Pruess, K., 2001. Modeling multiphase non-isothermal fluid flow and reactive geochemical transport in variably saturated fractured rocks: 1. Methodology. American Journal of Science, 301: 16-33.

Xu T., Sonnenthal, E., Spycher, N., Pruess, K., Brimhall, G., Apps, J., 2001. Modeling multiphase non-isothermal fluid flow and reactive geochemical transport in variably saturated fractured rocks: 2. Applications to supergene copper enrichment and hydrothermal flows. American Journal of Science, 301: 34-59.

Yang, I.C., Rattray, G.W., Yu, P., 1996. Interpretation of Chemical and Isotopic Data from Boreholes in the Unsaturated Zone at Yucca Mountain, Nevada. U.S. Geological Survey Water-Resources Investigations Report 96-4058. Denver, Colorado.